

Effect of Air-Pressure on Room Temperature Hydrogen Sensing Characteristics of Nanocrystalline Doped-Tin Oxide Mems-Based Sensor

Satyajit Shukla,¹ Lawrence Ludwig,² Hyoung J. Cho,¹ Julian Duarte,¹ and Sudipta Seal^{1,*}

¹Surface Engineering and Nano Fabrication Lab, Advanced Materials Processing and Analysis Center and Mechanical Materials, Aerospace Engineering Department, University of Central Florida, USA

²Kennedy Space Center, KSC-NASA, FL 32899, USA

Nanocrystalline indium oxide (In_2O_3)-doped tin oxide (SnO_2) thin film sensor has been sol-gel dip-coated on a microelectrochemical system (MEMS) device using a sol-gel dip-coating technique. Hydrogen (H_2) at ppm-level has been successfully detected at room temperature using the present MEMS-based sensor. The room temperature H_2 sensing characteristics (sensitivity, response and recovery time, and recovery rate) of the present MEMS-based sensor has been investigated as a function of air-pressure (50–600 Torr) with and without the ultraviolet (UV) radiation exposure. It has been demonstrated that, the concentration of the surface-adsorbed oxygen-ions (which is related to the sensor-resistance in air), the ppm-level H_2 , and the oxygen (O_2) partial pressure are the three major factors, which determine the variation in the room temperature H_2 sensing characteristics of the present MEMS-based sensor as a function of air-pressure.

Keywords: Air-Pressure, Hydrogen, MEMS, Nanocrystalline, Sensor, Tin Oxide.

1. INTRODUCTION

Hydrogen (H_2) has been considered as an alternative, cheap, and abundant fuel for heat generation by direct combustion or for power generation using solid oxide fuel cells (SOFCs). Transportation vehicles powered by SOFCs based on H_2 fuel are likely in near future.^{1,2} Moreover, liquid H_2 has been used to launch the space-vehicles. Due to the potential H_2 applications, research interest in H_2 technology has been escalated in recent years. Much attention has been paid for the production, storage, and transportation of H_2 in the gaseous as well as in the liquid forms.^{3–5} Due to an inflammable nature of H_2 , there is an immediate need for the development of highly efficient and low cost H_2 sensors operating under ambient conditions. Among different H_2 sensors available based on different operational principles,^{6–10} more attention has been by us towards improving the H_2 sensing ability of the nanocrystalline tin oxide (SnO_2) sensors based on the resistance change mechanism.^{11–13}

It is well known that, when a polycrystalline SnO_2 semiconductor thin film is exposed to air, physisorbed oxygen molecules pick-up electrons from the conduction band of SnO_2 and change to $\text{O}_{2\text{ads}}^-$ or O_{ads}^- species; thus, increasing the electrical resistance of the thin film. However, when a reducing gas, such as H_2 , comes in contact with the thin film, it gets oxidized via reaction with the $\text{O}_{2\text{ads}}^-$ or O_{ads}^- species, and subsequently, the electrons are reintroduced into the electron-depletion-layer leading to decrease in the electrical resistance of the thin film.¹⁴ The gas sensitivity (S) of the nanocrystalline SnO_2 thin film is usually determined by the ratio $R_{\text{air}}/R_{\text{gas}}$, where R_{air} and R_{gas} are the sensor-resistances in air without and with the reducing gas respectively.

The performance of a gas sensor is usually determined on the basis of its three fundamental properties—(i) sensitivity, (ii) response time, and (iii) recovery time. The role of nanocrystallite size,¹⁵ film thickness,¹⁶ operating temperature,¹⁷ nature and amount of dopants,^{18,19} surface-catalysts,²⁰ and surface-oxides²¹ on the H_2 sensing characteristics of SnO_2 -based sensors has been studied in the literature. However, all these investigations have

*Author to whom correspondence should be addressed.

been conducted in the higher operating temperature range ($>100\text{ }^{\circ}\text{C}$). Although there is a need for the development of room temperature H_2 sensors, such study in the lower operating temperature range ($<100\text{ }^{\circ}\text{C}$) is still lacking in the literature. Recently, we achieved the room temperature H_2 sensing with giant sensitivity, using the Pt-sputtered sol-gel derived nanocrystalline indium oxide (In_2O_3)-doped tin oxide (SnO_2) thin film sensor deposited on microelectromechanical systems (MEMS) device.^{12, 22} The effect of the sensor-exposure to the ultraviolet (UV) radiation on its room temperature H_2 sensitivity has also been reported.²² In our prior investigation,²² giant room temperature H_2 sensitivity has been demonstrated at lower air-pressure (50 Torr). However, the effect of higher range of air-pressure on the room temperature H_2 sensing characteristics of the present MEMS-based sensor is not yet determined. Since some of the potential H_2 applications (for example, space-based applications) require H_2 sensors to operate under different air-pressure conditions, it is essential to know the H_2 sensing characteristics of the present sensor as a function of air-pressure. Moreover, other applications, such as transportation vehicles, require H_2 sensors to operate under ambient atmospheric conditions (that is, higher air-pressure). Although the operating conditions for the H_2 sensors may change depending on the application, in the open literature, the effect of air-pressure on the room temperature H_2 sensing characteristics of SnO_2 -based sensors has not been discussed. In view of this, we study systematically the effect of air-pressure on the room temperature H_2 sensing characteristics of the In_2O_3 -doped SnO_2 thin film sensor sol-gel deposited on the MEMS device.

2. EXPERIMENTAL DETAILS

2.1. MEMS and Sensor Device Fabrication

To fabricate the MEMS-device with the interdigitated electrode configuration, the bare Pyrex glass slide was utilized as a substrate. During the fabrication, chromium (Cr, 10–20 nm) and gold (Au, 150–200 nm) thin films were deposited by thermal evaporation on the top of the bare Pyrex glass substrate. Four interdigitated electrodes and one temperature sensor were patterned on the substrate using the photolithography and the wet chemical etching techniques, Figure 1. Shipley 1400-27 positive photoresist was used for patterning the electrodes. In Figure 1, the gap between the Au electrodes is $20\text{ }\mu\text{m}$ for all four interdigitated electrode configurations. The fabricated MEMS device was utilized for the sol-gel dip-coating of the nanocrystalline In_2O_3 -doped SnO_2 thin films, and then, wire-bonded to a ceramic package for final H_2 sensing tests. The primary sensor test-board contained a 32 pin socket assembly, which was placed centered on the test-board. For the specific sensor-tests, the sensor-surface was exposed to the ultraviolet (UV) radiation emitted by light

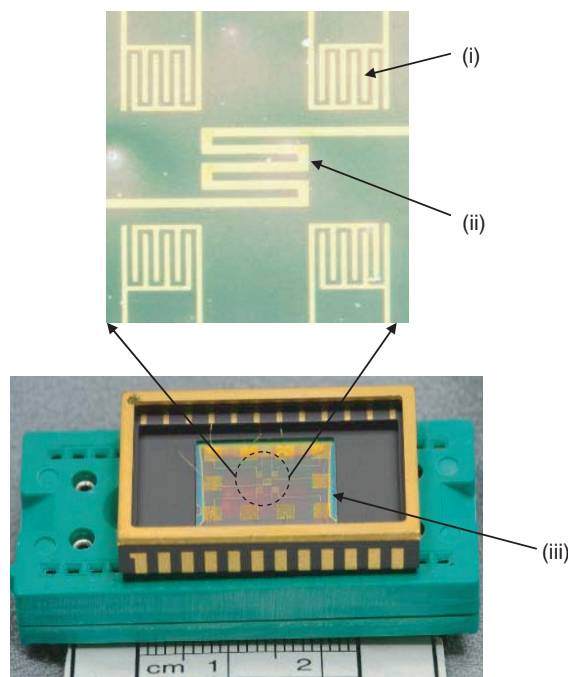


Fig. 1. MEMS-device, with the sol-gel dip-coated In_2O_3 -doped SnO_2 thin film sensor, is wire bonded to the integrated circuit chip mounted on a 32 pin socket assembly. The magnified view of an encircled portion is also shown, where four interdigitated Au electrode configurations with one resistive temperature sensor are visible. (i) interdigitated Au electrodes (electrode distance- $20\text{ }\mu\text{m}$), (ii) resistive temperature sensor, and (iii) MEMS device with Au pads.

emitting diode (LED) lamp, which was an InGaN LED mounted on lead frame with clear epoxy lens. On forward bias, it emitted a band of visible light that peaked 375 nm. Edge connectors facilitated the four-wire resistance-tests, which were used to characterize the sensor-test during an exposure to the specific amount of H_2 . A daughter-board was, then, fabricated using the same layout and prototyping software, which housed the UV-diode-lamp that was to be used to stimulate the sensor, as described in detail elsewhere.²² This daughter-board was installed using stand-off posts such that the UV-diode-lamp was mounted exactly on top of the sensor-surface.

2.2. Nanocrystalline Thin Film Sensor Deposition

Sol-gel dip-coating technique was utilized to deposit the nanocrystalline In_2O_3 -doped SnO_2 thin film sensor over the patterned MEMS device. For the sol-gel dip-coating process, tin(IV)-isopropoxide ($\text{Sn}[\text{OC}_3\text{H}_7]_4$) (10 w/v%) in iso-propanol (72 vol%) and toluene (18 vol%) and indium(III)-isopropoxide ($\text{Sn}[\text{OC}_3\text{H}_7]_3$) were purchased from Alfa Aesar (U.S.A.) and used as received. The solution of tin-isopropoxide in iso-propanol and toluene, corresponding to the concentration of 0.2–0.3 M of tin-isopropoxide, was prepared. Calculated amount of indium(III)-isopropoxide was dissolved in this solution to obtain the thin films containing 6.5 mol% In_2O_3 . The other

details related to the sol-gel dip-coating process have been provided elsewhere,²² and hence, not repeated here.

2.3. Characterization of MEMS-Based Nanocrystalline Thin Film Sensor

Focused ion beam (FIB) (200 TEM, FEI Company, Hillsboro, Oregon) milling technique was performed on the coated-MEMS device for preparing the transmission electron microscopy (TEM) specimen preparation. The procedure for the TEM sample preparation via FIB milling technique has been already described elsewhere.²³ The HRTEM analysis was then conducted (FEI-Philips Tecnai F30) to estimate the film thickness and the nanocrystallite size within the thin film sensor. Bright field HRTEM images at 300 kV were taken to observe the lattices. Selected-area electron diffraction (SAED) pattern was collected from the center of the sensing layer to analyze the crystal structure, which also provided the evidence for the presence of nanocrystals having different orientations within the sensor thin film. Energy dispersive spectroscopy (EDS) analysis was also carried out to determine the chemical constituents of the different layers observed in the HRTEM images as described later.

2.4. H₂ Sensing Tests

Before the start of the sensor-tests, the MEMS-based sensor was exposed to the UV-radiation with alternate 'ON' and 'OFF' states to confirm the response of the sensor to the UV-radiation. Under the UV-radiation, the room temperature resistance of the present MEMS-based sensor in air was decreased; while, without the UV-radiation, it was increased back to its original value.

The H₂ sensing-tests were, then, conducted in the dynamic test condition. In this type of sensor-testing, the original sensor-resistance was first stabilized in air at a given air-pressure (maintained using turbo-pumps) and at room temperature (22 °C). A mixture of nitrogen (N₂, used only as a carrier gas) and H₂ was admitted, through the respective mass-flow-controllers, into the test-chamber. A desired amount of H₂ (in ppm) was, thus, continuously blown into the test-chamber per minute and simultaneously pumped out of the test-chamber throughout the test-duration. Thus, the dynamic test condition simulated the condition, which may be encountered in an actual service application (for example, H₂ leakage through a pipe). All sensor-tests were conducted at room temperature (22 °C) with the total response time of 3600 sec. At the end, for the sensor-recovery, air at 760 Torr was blown into the test-chamber after making the turbo-pumps off. The initial air-pressure was, then, restored within few minutes by starting the turbo-pumps.

In contrast to our previous study,²² the dynamic sensor test in this investigation was conducted for a constant H₂ flow-rate of 3 sccm and for a constant 900 ppm level

H₂, with and without the UV-exposure, by varying the air-pressure within the range of 50–600 Torr.

3. RESULTS

3.1. HRTEM Analysis of MEMS-Based Sensor

Typical HRTEM images of the In₂O₃-doped SnO₂ thin film sensor, sol-gel dip-coated on the MEMS device are presented at different magnifications in Figure 2. Different layers have been identified using EDS analysis and are appropriately labeled in Figure 2. The Si, SiO₂, Au (pad), and Cr layers have been originated from the MEMS device fabrication process; on the other hand, Au-Pd and Pt layers have been created during the FIB milling procedure. An intermediate In₂O₃-doped SnO₂ layer having thickness 150 nm is clearly visible, Figures 2(a–c). At the highest magnification, Figure 2(d), this thin film sensor appears to be nanocrystalline in nature with the nanocrystallite size as small as 1–3 nm. The SAED pattern (see the inset in Fig. 2(d)) obtained from the region-iv shows continuous and sharp ring pattern suggesting the nanocrystalline nature of the thin film sensor.

3.2. Effect of Air-Pressure on Stabilized Sensor-Resistance in Air

The variation in the stabilized sensor-resistance in air (without H₂) as a function of air-pressure within the range of 50–600 Torr, without and with the UV-exposure, is presented in Figure 3. Without the UV-exposure, the stabilized sensor-resistance in air is observed to be as high

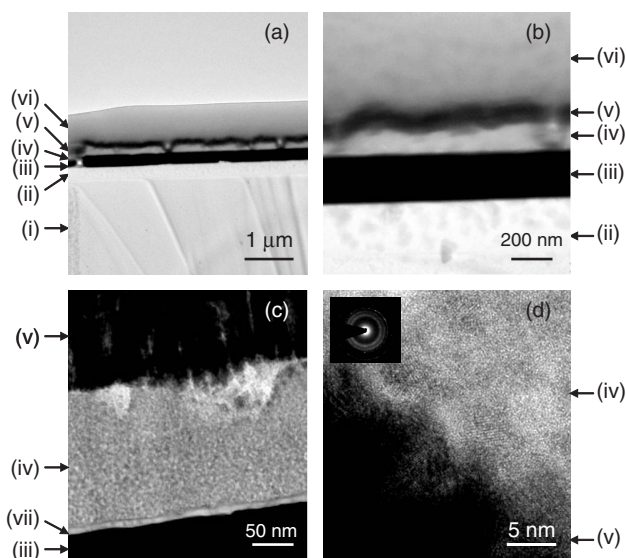


Fig. 2. HRTEM images of In₂O₃-doped SnO₂ thin film sensor, sol-gel dip-coated on the MEMS device, obtained at different magnifications using the FIB-milled specimen. (i) Si, (ii) SiO₂, (iii) Au pad, (iv) In₂O₃-doped SnO₂, (v) Au-Pd, (vi) Pt, and (vii) Cr. Inset in (d) is a SAED pattern obtained from the region-iv.

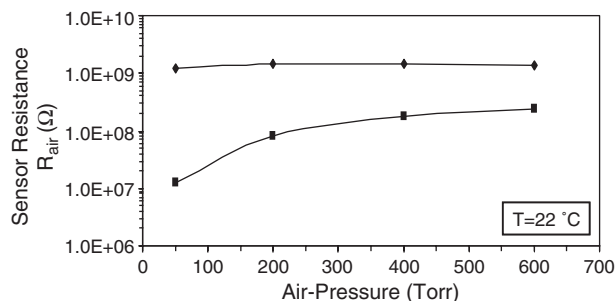


Fig. 3. Variation in the stabilized room temperature sensor-resistance in air as a function of air-pressure. \blacklozenge -UV-OFF \blacksquare -UV-ON.

as 1.5 G Ω and almost independent of the air-pressure within the investigated range. However, the stabilized room temperature sensor-resistance is noted to be lower under the UV-exposure within the investigated air-pressure range. Typically at 50 Torr air-pressure, under the UV-radiation, the stabilized sensor-resistance in air drops down to 15 M Ω , Figure 3. Moreover, the stabilized sensor-resistance in air is observed to increase with increasing air-pressure under this condition; however, the slope is noted to decrease with increasing air-pressure, which indicates the saturation of the stabilized sensor-resistance in air in the higher air-pressure range. Thus, the variation in the sensor-resistance in air, as a function of air-pressure, is observed to be different without and with the UV-radiation.

3.3. Effect of Air-Pressure on Sensor-Resistance in Air with H₂

Typical variation in the sensor-resistance as a function of time, in the presence of air containing H₂, is presented in Figures 4 and 5, where H₂ is admitted into the test-chamber at a constant flow-rate of 3 sccm at 200 Torr and at constant 900 ppm level at 400 Torr air-pressure respectively. The sensor-tests in Figures 4(a)–5(a) and Figures 4(b)–5(b) are conducted without and with the UV-exposure respectively. Upon the admission of H₂ into the test-chamber, a continuous drop in the sensor-resistance is noted. A significant sensor-resistance drop of three- to five-orders of magnitude is observed after the total test duration of 3600 sec. The sensor-resistance recovers quickly after blowing the air at 760 Torr under all test-conditions.

3.4. Effect of Air-Pressure on Room Temperature H₂ Sensitivity

Typical variation in the room temperature H₂ sensitivity as a function of time for different air-pressure levels within the range of 50–600 Torr, without and with the UV-exposure, is presented in Figures 6(a) and 6(b) respectively, where the sensor-tests are conducted for a constant H₂ flow-rate of 3 sccm. Without the UV-exposure, Figure 6(a), the room temperature H₂ sensitivity is noted to

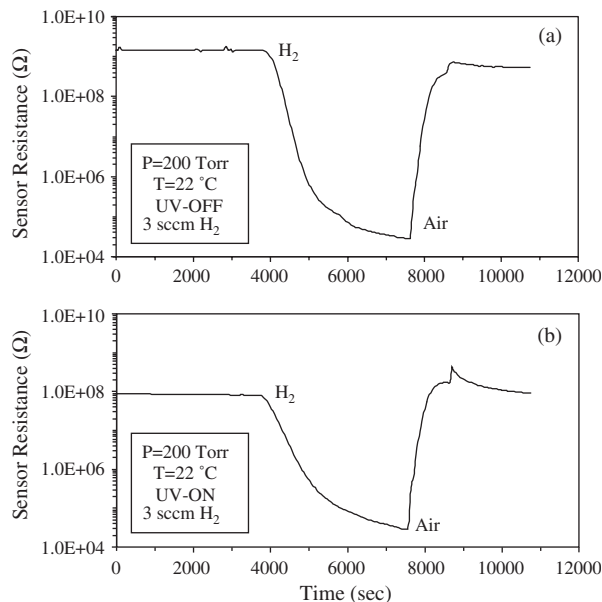


Fig. 4. Variation in the room temperature sensor-resistance as a function of time. H₂ is blown, at a constant flow rate of 3 sccm, into the test-chamber containing air at 200 Torr for the total response time of 3600 sec. Air at 760 Torr is blown into the test-chamber for the recovery of the sensor-resistance.

increase with increasing test-duration. However, depending on the air-pressure, a minimum response time is required before an increase in the H₂ sensitivity is noted. The minimum response time is observed to increase with increasing air-pressure. Moreover, the rate of increase in the room temperature H₂ sensitivity is also observed to be a function of the air-pressure, and it decreases with

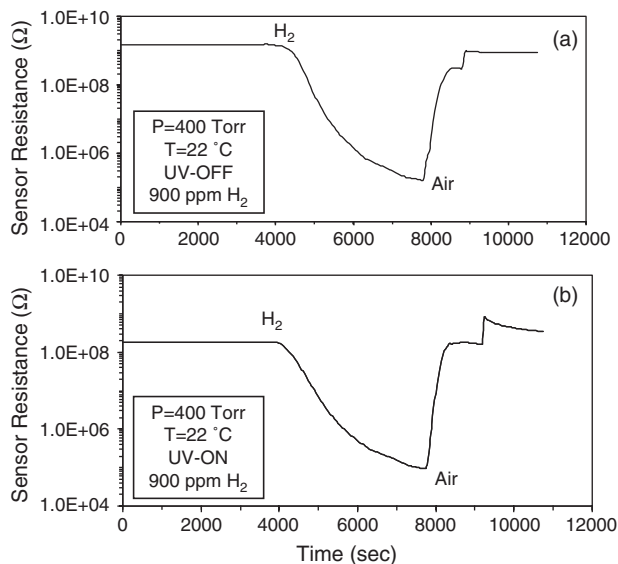


Fig. 5. Variation in the room temperature sensor-resistance as a function of time. A constant 900 ppm H₂ is blown per minute into the test-chamber containing air at 400 Torr for the total response time of 3600 sec. Air at 760 Torr is blown into the test-chamber for the recovery of the sensor-resistance.

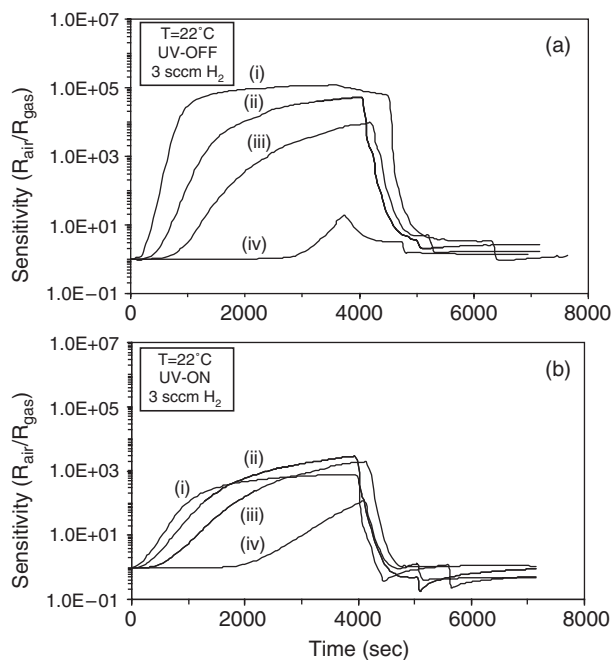


Fig. 6. Variation in the room temperature H_2 sensitivity of the present MEMS-based sensor as a function of time. (i) 50 Torr, (ii) 200 Torr, (iii) 400 Torr, and (iv) 600 Torr air-pressure. The sensor-tests are conducted for a constant H_2 flow rate of 3 sccm.

increasing air-pressure. The room temperature H_2 sensitivity is observed to saturate, within the total test-duration of 3600 sec, only for the lowest air-pressure investigated (50 Torr). However, in the higher air-pressure range, the steady-state H_2 sensitivity value is not achieved within the above test-duration. Further, the maximum room temperature H_2 sensitivity is observed to be a function of air-pressure, and it decreases with increasing air-pressure. The maximum room temperature H_2 sensitivity decreases from 10^5 to 10^1 as the air-pressure increases from 50–600 Torr. The room temperature H_2 sensitivity decreases rapidly from the maximum value under all test-conditions after blowing the air into the test-chamber at 760 Torr.

In Figure 6(b), where the sensor-tests are conducted under the UV-radiation, the maximum room temperature H_2 sensitivity (45 to 2.4×10^3) is observed to be a function of air-pressure. The variation in the room temperature H_2 sensitivity as a function of test-duration is more or less similar to that observed in Figure 6(a), except that the maximum room temperature H_2 sensitivity for 50 Torr air-pressure is less than that observed for higher air-pressures (200 and 400 Torr). Comparison of Figures 6(a) and 6(b) shows that, at a given air-pressure, the rate of increase in the room temperature H_2 sensitivity is larger without the UV-exposure than that with the UV-exposure; although the minimum response time is observed to be lesser with the UV-exposure. Further comparison reveals that, the UV-exposure reduces the maximum room temperature H_2 sensitivity for the air-pressure values within the range of 50–400 Torr. This trend is, however, reversed at the highest

air-pressure of 600 Torr. At this air-pressure, the maximum room temperature H_2 sensitivity is larger with the UV-exposure than that without the UV-exposure.

Typical variation in the room temperature H_2 sensitivity as a function of test-duration for different air-pressures, without and with the UV-exposure, is presented in Figures 7(a) and 7(b) respectively for the sensor-tests conducted at a fixed H_2 concentration of 900 ppm (a constant ppm-level test). In Figure 7(a), the maximum room temperature H_2 sensitivity is noted to lie within the narrow range of 6×10^4 – 10^5 ; while in Figure 7(b), it lies within the relatively broader range of 770 – 3×10^4 . Comparison of Figures 7(a) and 7(b) reveals a decrease in the maximum room temperature H_2 sensitivity under the UV-exposure within the investigated air-pressure range. Comparison of Figures 6(a) and 7(a) shows that, for a constant 900 ppm H_2 , the air-pressure has almost no effect on the minimum response time, the rate of increase in the room temperature H_2 sensitivity, and the maximum room temperature H_2 sensitivity. However, under the UV-exposure for a constant ppm-level test, Figure 7(b), the maximum room temperature H_2 sensitivity is observed to depend on the air-pressure. Interestingly, the room temperature H_2 sensitivity under the UV-exposure is noted to increase with increasing air-pressure; this trend is, however, almost reversed for a constant H_2 flow-rate of 3 sccm, Figure 6(b). It is also noted that, for the sensor-tests conducted for a constant 900 ppm H_2 within the investigated air-pressure range of 50–600 Torr, Figure 7, the room temperature H_2 sensitivity saturates within a short duration although the total test-duration is 3600 sec.

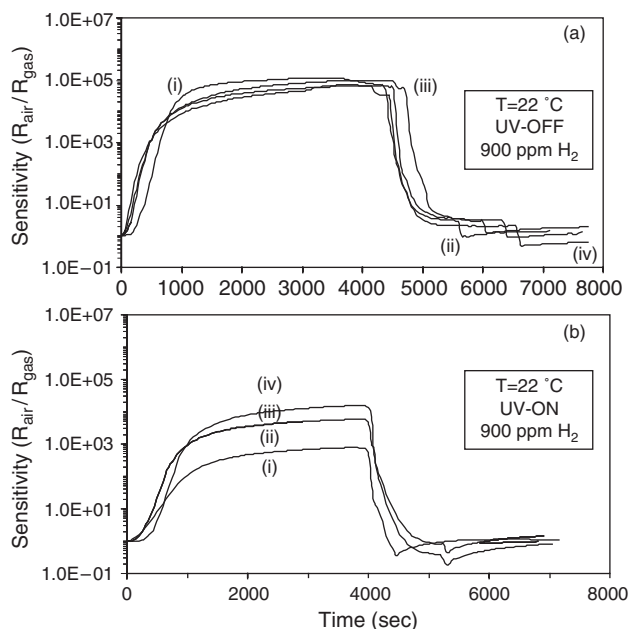


Fig. 7. Variation in the room temperature H_2 sensitivity of the present MEMS-based sensor as a function of time. (i) 50 Torr, (ii) 200 Torr, (iii) 400 Torr, and (iv) 600 Torr air-pressure. The sensor-tests are conducted for a constant 900 ppm H_2 .

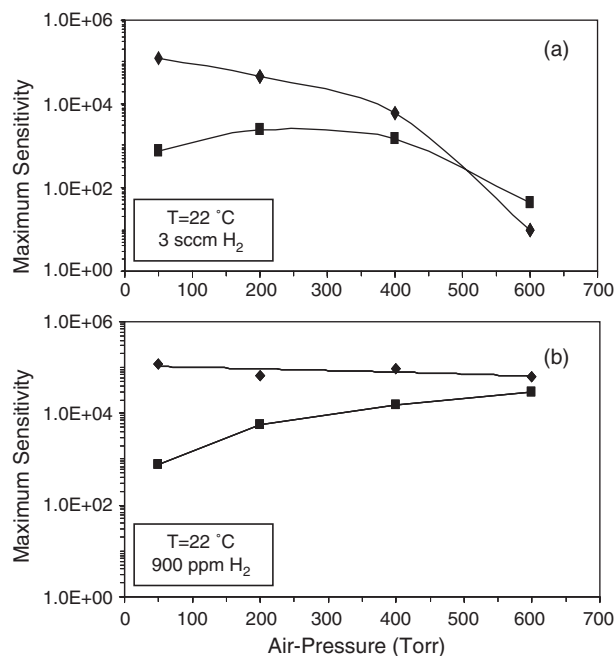


Fig. 8. Variation in the maximum room temperature H₂ sensitivity of the present MEMS-based sensor as a function of air-pressure. ◆-UV-OFF and ■-UV-ON.

The maximum room temperature H₂ sensitivity, observed without and with the UV-exposure, is compared in Figures 8(a) and 8(b), for the sensor-tests conducted for a constant H₂ flow-rate of 3 sccm and a constant 900 ppm H₂ respectively. In Figure 8(a), the maximum room temperature H₂ sensitivity, without the UV-exposure, is observed to decrease from 10⁵ to 10¹ with increasing air-pressure. However, under the UV-radiation, the maximum room temperature H₂ sensitivity increases first from 770 to 2.4 × 10³ and then decreases to 45 with increasing air-pressure. Except at the highest air-pressure (600 Torr), the maximum room temperature H₂ sensitivity is higher without the UV-exposure than that with the UV-exposure. On the other hand, in Figure 8(b), for a constant 900 ppm H₂, the maximum room temperature H₂ sensitivity without the UV-exposure decreases marginally from 10⁵ to 6 × 10⁴; while, under the UV-radiation, it increases from 770 to 3 × 10⁴ with increasing air-pressure. Under these test-conditions, the maximum room temperature H₂ sensitivity is observed to be higher without the UV-exposure than that with the UV-exposure within the investigated air-pressure range. In Figure 8, for both the test-conditions, the difference in the maximum room temperature H₂ sensitivities, without and with the UV-exposure, is noted to decrease with increasing air-pressure.

3.5. Effect of Air-Pressure on Room Temperature Response and Recovery Time

The variation in the response time as a function of air-pressure, observed for a constant H₂ flow-rate of 3 sccm

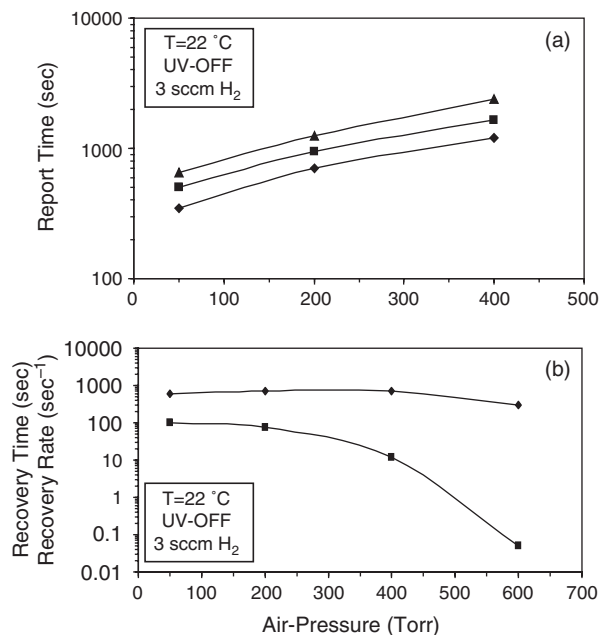


Fig. 9. (a) Variation in the room temperature response time of the present MEMS-based sensor as a function of air-pressure for the different H₂ sensitivity levels. ◆-10 ■-100 ▲-1000. (b) Variation in the room temperature recovery rate (■) and recovery time (◆) as a function of air-pressure. The recovery time corresponds to the time required to reduce the H₂ sensitivity from the maximum value to 5, which corresponds to the almost linear drop in the sensor-resistance in Figure 6(a).

without the UV-exposure, for different room temperature H₂ sensitivity levels, is presented in Figure 9(a). For all room temperature H₂ sensitivity levels, the response time increases with increasing air-pressure. The response time lies within the range of 300–2400 sec for the room temperature H₂ sensitivity within the range of 10–1000 as the air-pressure varies within the range 50–600 Torr. The rate of increase in the response time with respect to the air-pressure is not affected by the different room temperature H₂ sensitivity levels. The variation in the recovery rate (defined as the ratio of ΔS and Δt , where ΔS is the difference between the maximum and lower room temperature H₂ sensitivity levels, and Δt the time required for decreasing the room temperature H₂ sensitivity by ΔS during the recovery process) and the recovery time as a function of air-pressure, observed for a constant H₂ flow-rate of 3 sccm without the UV-exposure, is presented in Figure 9(b). The recovery rate is observed to decrease continuously with increasing air-pressure. The recovery rate decreases from 100 sec⁻¹ to 0.05 sec⁻¹ as the air-pressure increases from 50 to 600 Torr. The rate of decrease in the recovery rate is observed to increase with increasing air-pressure. This nature of the variation in the recovery rate, Figure 9(b), is very similar to that in the maximum room temperature H₂ sensitivity as a function of air-pressure, Figure 8(a), observed under similar test-conditions. The recovery time, on the other hand, is observed to be almost

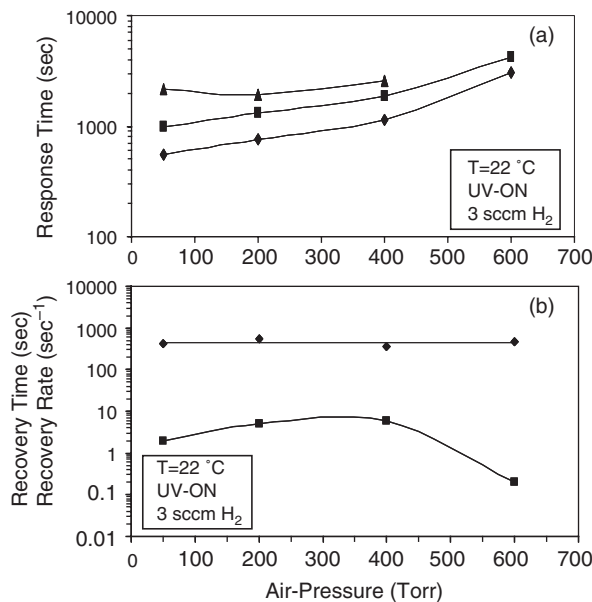


Fig. 10. (a) Variation in the room temperature response time of the present MEMS-based sensor as a function of air-pressure for the different H_2 sensitivity levels. \blacklozenge -10 \blacksquare -100 \blacktriangle -500. (b) Variation in the room temperature recovery rate (\blacksquare) and recovery time (\blacklozenge) as a function of air-pressure. The recovery time corresponds to the time required to reduce the H_2 sensitivity from the maximum value to 1 in Figure 6(b).

constant and lies within the narrow range of 300–720 sec for the investigated air-pressure range.

The variation in the response time as a function of air-pressure, observed for a constant H_2 flow-rate of 3 sccm with the UV-exposure, is presented in Figure 10(a). In general, for different room temperature H_2 sensitivity levels, the response time tends to increase with increasing air-pressure. This trend is similar to that observed in Figure 9(a). The response time lies within the range of 540–3600 sec for the room temperature H_2 sensitivity range of 10–500 as the air-pressure varies from 50 to 600 Torr. The variation in the recovery rate and the recovery time as a function of air-pressure, observed for a constant H_2 flow-rate of 3 sccm under the UV-radiation, is presented in Figure 10(b). The recovery rate is first observed to increase from 2 sec^{-1} to 6 sec^{-1} as the air-pressure increases within the range of 50–400 Torr. The recovery rate, however, decreases to 0.2 sec^{-1} at the highest air-pressure. This variation in the recovery rate, Figure 10(b), is very similar to that in the room temperature H_2 sensitivity, Figure 8(a), as a function of air-pressure, observed for a constant H_2 flow-rate of 3 sccm with the UV-exposure. The recovery time, on the other hand, is observed to be almost constant and varies within the narrow range of 420–540 sec for the investigated range of air-pressure.

The variation in the response time, recovery rate, and recovery time as a function of air-pressure for a constant 900 ppm H_2 , without and with the UV-exposure, is presented in Figures 11 and 12 respectively. In Figures 11(a)

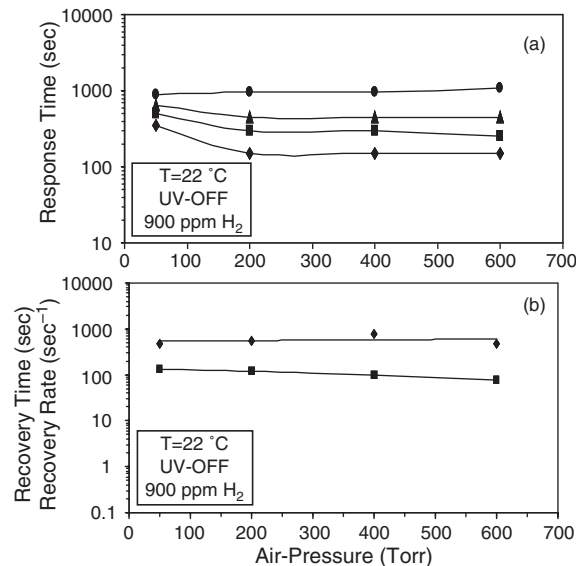


Fig. 11. (a) Variation in the room temperature response time of the present MEMS-based sensor as a function of air-pressure for the different H_2 sensitivity levels. \blacklozenge -10 \blacksquare -100 \blacktriangle -1000, \bullet -10000. (b) Variation in the room temperature recovery rate (\blacksquare) and recovery time (\blacklozenge) as a function of air-pressure. The recovery time corresponds to the time required to reduce the H_2 sensitivity from the maximum value to 5, which corresponds to the almost linear drop in the sensor-resistance in Figure 7(a).

and 12(a), the response time is observed to be nearly independent of the air-pressure and lies within the range of 180–960 sec and 420–1020 sec respectively for the room temperature H_2 sensitivity range of 10 – 10^4 and 10 – 10^3

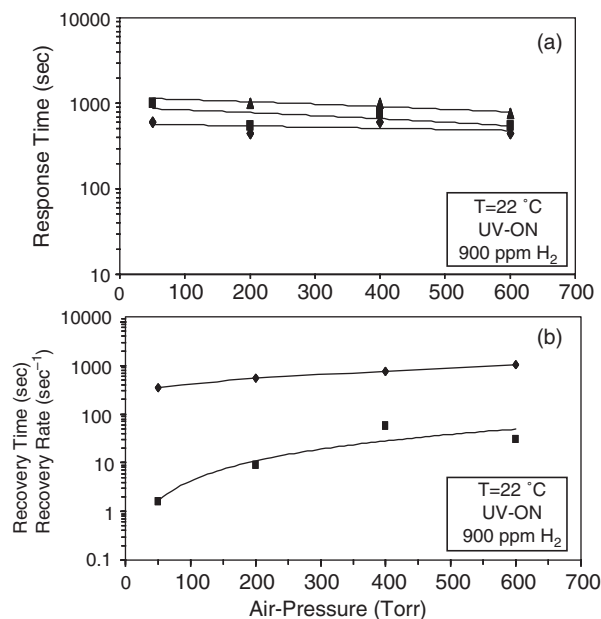


Fig. 12. (a) Variation in the room temperature response time of the present MEMS-based sensor as a function of air-pressure for the different H_2 sensitivity levels. \blacklozenge -10 \blacksquare -100 \blacktriangle -1000. (b) Variation in the room temperature recovery rate (\blacksquare) and recovery time (\blacklozenge) as a function of air-pressure. The recovery time corresponds to the time required to reduce the H_2 sensitivity from the maximum value to 1 in Figure 7(b).

respectively. In Figures 11(b) and 12(b), the recovery rate is observed to decrease from 130 sec^{-1} to 75 sec^{-1} and to increase from 1.5 sec^{-1} to 55 sec^{-1} respectively with increasing air-pressure. This variation in the recovery rate, without and with the UV-exposure, is very similar to that in the maximum room temperature H_2 sensitivity observed under the respective test-conditions, Figure 8(b). Thus, for the sensor-tests conducted with a constant H_2 flow-rate of 3 sccm and a constant 900 ppm H_2 , the variation in the recovery rate as a function of air-pressure follows the same trend as exhibited by the variation in the maximum room temperature H_2 sensitivity as a function of air-pressure. In Figures 11(b) and 12(b), the recovery time measured for the sensor-tests conducted without and with the UV-exposure, is noted in between 480–780 sec and 360–1000 sec respectively as the air-pressure increases from 50 to 600 Torr. The recovery time, without the UV-exposure (Fig. 11(b)), is observed to decrease marginally with increasing air-pressure; while, that with the UV-exposure (Fig. 12(b)), is noted to increase with increasing air-pressure.

4. DISCUSSION

Sol-gel derived nanocrystalline In_2O_3 -doped SnO_2 thin film sensor has been incorporated into the MEMS device. Under the given processing conditions, the nanocrystalline thin film sensor has 150 nm thickness with 1–3 nm nanocrystallite size, which are optimum to sense H_2 at room temperature. In the present investigation, H_2 has been successfully sensed at room temperature by using the present nanocrystalline MEMS-based sensor with giant room temperature H_2 sensitivity as high as 10^5 . It is further shown that, the room temperature H_2 sensitivity, the response and the recovery time, and the recovery rate of the present MEMS-based sensor are strongly affected by the variation in the air-pressure, with and without the UV-exposure, which requires further attention.

4.1. Effect of Air-Pressure on Room Temperature H_2 Sensitivity

The present sensor, in the as synthesized condition, exhibits extremely high resistance ($1.5 \text{ G}\Omega$) in air, which is independent of the air-pressure within the investigated range (Fig. 3). Since, the sensor-resistance in air is primarily determined by the concentration of the surface-adsorbed oxygen-ions,²⁴ it appears that, within the investigated air-pressure range, the concentration of the surface-adsorbed oxygen-ions is not affected by the variation in the air-pressure without the UV-exposure. However, when the sensor-surface is exposed to the UV-radiation, desorption of the surface-adsorbed oxygen-ions from the sensor-surface is likely to occur in the form of gaseous O_2 molecules.²² During this desorption process, electrons are reintroduced

into the conduction band of doped- SnO_2 , which may reduce the grain-boundary potential-barrier for the electron conduction; thus, decreasing the sensor-resistance in air. The sensor-resistance under the UV-radiation is, hence, noted to be less than that without the UV-exposure within the entire investigated air-pressure range (Fig. 3).

Moreover, in contrast to the behavior noted without the UV-exposure, the sensor-resistance in air is observed to increase with increasing air-pressure under the UV-radiation, which suggests that, the concentration of the surface-adsorbed oxygen-ions increases with increasing air-pressure under the UV-radiation. Thus, the concentration of the surface-adsorbed oxygen-ions appears to be independent of the air-pressure without the UV-exposure; however, it increases with increasing air-pressure under the UV-radiation. It seems that, at room temperature, the energy supplied by the UV-radiation reduces the sensor-resistance by desorbing the surface-adsorbed oxygen-species. On the other hand, increasing air-pressure progressively results in more oxygen-ion adsorption on the sensor-surface, which tends to reduce the effect of the UV-exposure. As a result of the competition between the effects of UV-exposure and increasing air-pressure, the variation in the room temperature sensor-resistance becomes more sensitive to the variation in the air-pressure under the UV-radiation than that without the UV-radiation (Fig. 3). With the UV-exposure, the effect of UV-radiation dominates at lower air-pressure while the effect of air-pressure dominates in higher air-pressure range.

The variation in the surface-adsorbed oxygen-ion concentration as a function of air-pressure is one of the three major factors, which determine the observed variation in the room temperature H_2 sensitivity of the present MEMS-based sensor as a function of air-pressure. Recently, we proposed a new constitutive equation for the gas sensitivity of semiconductor oxides sensors,^{25–27} which is of the form,

$$S = A_1 \cdot \frac{2d}{D} \cdot \frac{C^n}{n_b} \cdot \exp\left[\frac{q^2}{2\varepsilon_r\varepsilon_0k} \cdot \frac{[O^-]^2}{[V_o]T}\right] \quad (1)$$

where, A_1 is a constant (m^{-3}), d the space-charge-layer thickness, D the nanocrystallite size, C the gas concentration, n_b the bulk charge-carrier-density, q the electronic charge, $\varepsilon_r\varepsilon_0$ the permittivity of the sensor, $[O^-]$ the surface-density of states, $[V_o]$ the oxygen-ion-vacancy concentration, and T the operating temperature. The constitutive equation predicts that, at a given operating temperature, the increasing concentration of the surface-adsorbed oxygen-ions (that is, increasing sensor-resistance in air) should enhance the H_2 sensitivity and vice a versa, which is also demonstrated experimentally by others.^{16, 28}

In addition to the concentration of the surface-adsorbed oxygen-ions, the dependence of the room temperature H_2 sensitivity on the air-pressure and the UV-exposure (Fig. 8)

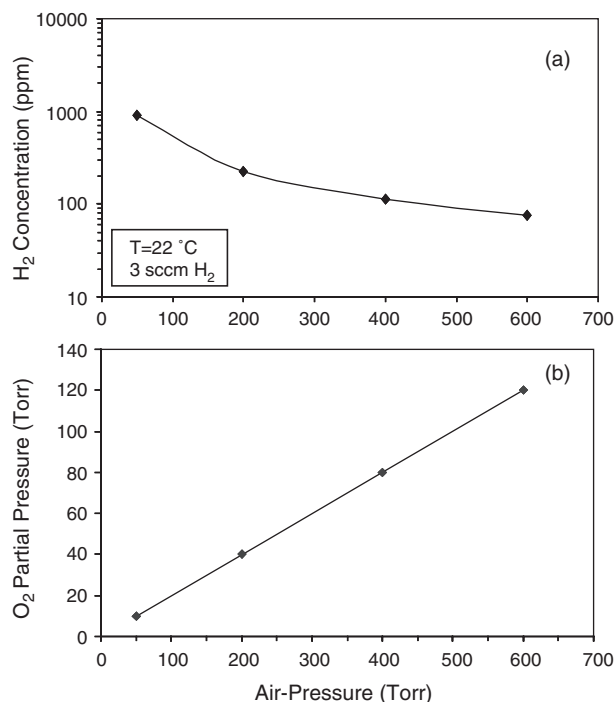


Fig. 13. Variation in the H₂ concentration (a) and the O₂ partial pressure (b) as a function of air-pressure.

is also governed by two other factors—(i) the H₂ concentration (ppm-level) and (ii) the O₂ partial pressure. As shown in Figure 13(a), with increasing air-pressure, within the range of 50–600 Torr, the H₂ concentration decreases from 900 ppm to 76 ppm for a constant flow-rate of 3 sccm. The reduced H₂ sensitivity with the decreasing H₂ ppm-level has been reported at higher as well as at lower operating temperature ranges for SnO₂-based sensors.^{18,22} As a result, for a constant flow-rate test, the decreasing H₂ ppm-level with increasing air-pressure, would tend to reduce the room temperature H₂ sensitivity of the present MEMS-based sensor. Moreover, as shown in Figure 13(b), the O₂ partial pressure increases with increasing air-pressure, which would also tend to reduce the room temperature H₂ sensitivity of the present MEMS-based sensor.²⁹ It appears that, the observed variation in the room temperature H₂ sensitivity as a function of air-pressure and the UV-exposure (Fig. 8) can be well explained on the basis of the above three critical parameters. It is to be, however, noted that, for the sensor-tests conducted for a constant ppm-level, the variation in the room temperature H₂ sensitivity of the present MEMS-based sensor as a function of air-pressure does not depend on the H₂ ppm-level. Hence, the concentration of the surface-adsorbed oxygen-ions, the H₂ ppm-level, and the O₂ partial pressure are the three important factors to be considered for a constant flow-rate test; while, the concentration of the surface-adsorbed oxygen-ions and the O₂ partial pressure are only to be considered for a constant ppm-level test.

In Figure 8(a), the room temperature H₂ sensitivity, without the UV-exposure, is observed to decrease with increasing air-pressure for a constant H₂ flow-rate of 3 sccm. Since, without the UV-exposure, the concentration of the surface-adsorbed oxygen-ions is independent of the air-pressure (Fig. 3), this suggests that, the concentration of the surface-adsorbed oxygen-ions has no effect on the variation in the room temperature H₂ sensitivity of the present MEMS-based sensor as a function of air-pressure. Hence, the observed decrease in the room temperature H₂ sensitivity as a function of increasing air-pressure, without the UV-exposure, appears to be a result of decreasing H₂ ppm-level and increasing O₂ partial pressure (Fig. 13). Interestingly, the room temperature H₂ sensitivity measured using a constant ppm-level test, without the UV-exposure, decreases only marginally with increasing air-pressure (Fig. 8(b)). Since, under these test-conditions, the H₂ ppm-level does not affect the variation in the room temperature H₂ sensitivity as a function of air-pressure, this suggests that, for the sensor-tests conducted without the UV-exposure, the O₂ partial pressure too has relatively smaller effect on the room temperature H₂ sensitivity of the present MEMS-based sensor. Thus, the sensor-tests conducted without the UV-exposure suggests that, both the surface-adsorbed oxygen-ions and the O₂ partial pressure do not significantly affect on the room temperature H₂ sensitivity of the present MEMS-based sensor. Hence, the decreasing room temperature H₂ sensitivity with increasing air-pressure, observed without the UV-exposure for a constant flow-rate test (Fig. 8(a)), is primarily attributed to the decreasing H₂ ppm-level with increasing air-pressure. On the other hand, a marginal decrease in the room temperature H₂ sensitivity with increasing air-pressure, observed without the UV-exposure for a constant ppm-level test (Fig. 8(b)), is attributed to the minor effect of increasing O₂ partial pressure.

The relative importance of the concentration of the surface-adsorbed oxygen-ions, the H₂ ppm-level, and the O₂ partial pressure on the room temperature H₂ sensitivity is also evident from the sensor-tests conducted under the UV-radiation. The room temperature H₂ sensitivity measured under the UV-radiation, for a constant flow-rate test (Fig. 8(a)), is noted to increase first with the air-pressure. This initial rise in the room temperature H₂ sensitivity is caused by the increased concentration of the surface-adsorbed oxygen-ions as suggested by the increasing sensor-resistance with the air-pressure under the UV-radiation (Fig. 3). However, under these test-conditions, the sensor-resistance, and hence, the concentration of the surface-adsorbed oxygen-ions, tend to saturate in the higher air-pressure range. As a result, the effect of decreasing H₂ ppm-level and increasing O₂ partial pressure (Fig. 13) dominates in the higher air-pressure range, which causes the room temperature H₂ sensitivity of the present MEMS-based sensor to decrease (Fig. 8(a)) under

the UV-radiation. Interestingly, the room temperature H_2 sensitivity measured at a constant H_2 ppm-level, under the UV-radiation, increases continuously with the air-pressure (Fig. 8(b)). Since H_2 ppm-level does not affect the variation in the room temperature H_2 sensitivity as a function of air-pressure under these test-conditions, this suggests that, the O_2 partial pressure has relatively smaller effect on the room temperature H_2 sensitivity under the UV-radiation as well. From the overall analysis, it appears that, the increasing room temperature H_2 sensitivity as observed in Figure 8, is a result of increasing concentration of the surface-adsorbed oxygen-ions; while, the decreasing room temperature H_2 sensitivity is mainly contributed by the decreasing H_2 ppm level and partly by increasing O_2 partial pressure as a function of increasing air-pressure.

4.2. Effect of Air-Pressure on Response and Recovery Time

For a constant H_2 flow-rate test, the response time of the present MEMS-based sensor, for different room temperature H_2 sensitivity levels, is observed to increase with the air-pressure, without (Fig. 9(a)) and with (Fig. 10(a)) the UV-exposure. As in the previous case, the concentration of the surface-adsorbed oxygen-ions, the H_2 ppm-level, and the O_2 partial pressure are the three critical parameters, which significantly affect the response time of the present MEMS-based sensor. In general, the increasing concentration of the surface-adsorbed oxygen-ions as a function of air-pressure is conducive to reduce the response time; while, the decreasing H_2 ppm-level and increasing O_2 partial pressure would tend to increase the response time for a given room temperature H_2 sensitivity level. It is to be noted that, such variation in the response time as a function of air-pressure for the different H_2 sensitivity levels is important to be known since different H_2 applications may consider different H_2 sensitivity values as a minimum level to generate a leak alarm.

Although the variation in the concentration of the surface-adsorbed oxygen-ions in air as a function of air-pressure is different, with and without the UV-exposure (Fig. 3), the response time always tends to increase with the air-pressure under these test-conditions (Figs. 9(a) and 10(a)). As a result, it appears that, the surface-adsorbed oxygen-ions do not have any significant effect on the response time, within the selected air-pressure range, for both with and without the UV-exposure. Hence, the increasing response time with increasing air-pressure, observed without (Fig. 9(a)) and with (Fig. 10(a)) the UV-exposure, is primarily attributed to the decreasing H_2 ppm-level and increasing O_2 partial pressure as a function of air-pressure.

Interestingly, almost constant response time has been observed for different room temperature H_2 sensitivity levels as a function of increasing air-pressure (Figs. 11(a) and 12(a)), when the sensor-tests are conducted at a constant

ppm-level. Since, under these test-conditions, H_2 ppm-level has no influence on the response time, this further suggests that, the O_2 partial pressure has a negligible or no effect on the response time of the present MEMS-based sensor. Hence, the increasing response time with increasing air-pressure, observed for a constant H_2 flow-rate, without and with the UV-exposure (Figs. 9(a) and 10(a)), is attributed to the decreasing H_2 ppm-level only.

The recovery time of the present MEMS-based sensor has been observed to remain nearly constant as a function of air-pressure under almost all test-conditions (Figs. 9–12). However, the recovery rate (which is a function of the rate of surface-adsorption of oxygen-ions from the surrounding atmosphere) has been noted to vary significantly as a function of air-pressure. Moreover, the nature of the variation in the recovery rate as a function of air-pressure depends on the test-conditions. It is noted that, under all similar test-conditions, the change in the recovery rate as a function of air-pressure (Figs. 9(b)–12(b)) follows the same trend as exhibited by the change in the maximum room temperature H_2 sensitivity as a function of air-pressure (Fig. 8). The recovery rate is, hence, associated with the maximum room temperature H_2 sensitivity and vice a versa; and as a result, the recovery time remains constant under all test-conditions.

Lastly, it is noted that, for the constant H_2 sensitivity levels, the present MEMS-based sensor shows minimum response time without the UV-radiation than that with the UV-exposure, which is in consonance with our earlier investigation.²² Conversely, for a given response time, it exhibits higher H_2 sensitivity without the UV-radiation than that with the UV-exposure. The recovery rate is also observed to be higher without the UV-radiation than that with the UV-exposure. Hence, the room temperature H_2 sensing characteristics of the present MEMS-based sensor are superior without the UV-radiation within the investigated air-pressure range. However, there are two major benefits associated with the sensor-exposure to the UV-radiation, which are lost its absence. First, the exposure to the UV-radiation has been reported to burn the organic residue present on the sensor-surface.³⁰ This provides a clean sensor-surface for sensing H_2 at room temperature; thus, improving its functionality. Second, the baseline sensor-resistance under the UV-exposure is observed to be much lower than that without the UV-radiation (Fig. 3). This could be advantageous since it makes possible to monitor the sensor-resistance by using a conventional low cost electronics instead of using a picamp, which may be needed to measure the higher sensor-resistance values (1 G Ω) in the absence of UV-exposure.

5. CONCLUSIONS

- (1) H_2 at ppm-level has been successfully sensed at room temperature, using the present MEMS-based sensor, with very high sensitivity (as high as 10^5) and the

response and the recovery times of few minutes. The room temperature H₂ sensing characteristics of the present MEMS-based sensor make it suitable to detect H₂ leakages in various practical applications involving the production, storage, transportation, and the use of gaseous and liquid forms of H₂.

- (2) The room temperature H₂ sensitivity of the present MEMS-based sensor, with and without the UV-exposure, is a function of the air-pressure within the investigated range of 50–600 Torr.
- (3) The observed trend in the variation in the room temperature H₂ sensitivity as a function of air-pressure, with and without the UV-exposure, is an optimum balance between the increasing room temperature H₂ sensitivity due to the increasing concentration of the surface-adsorbed oxygen-ions (as indicated the increasing original sensor-resistance in air) and the decreasing room temperature H₂ sensitivity mainly due to the decreasing H₂ ppm-level and partly due to the increasing O₂ partial pressure as a function of air-pressure.
- (4) The room temperature response time of the present MEMS-based sensor is dependent primarily on the H₂-ppm level within the investigated air-pressure range. The concentration of the surface-adsorbed oxygen-ions and the O₂ partial pressure do not significantly affect the response time of the present MEMS-based sensor.
- (5) The room temperature recovery rate of the present MEMS-based sensor is a function of its room temperature H₂ sensitivity. As a result, the room temperature recovery rate is observed to increase with increasing room temperature H₂ sensitivity and vice versa. As a consequence, the room temperature recovery time of the present MEMS-based sensor is almost independent of the air-pressure within the investigated range.

Acknowledgments: The authors thank UCF, Florida Space Grant Consortium (FSGC), NASA-Glenn (NASA NAG 32751), KSC-NASA, National Science Foundation (NSF EEC-0136710 and NSF CTS 0350572) (Seal) and (NSF CAREER, ECS-0348603 (Cho)) for funding the sensor and the nano-technology research.

References and Notes

1. J. M. Ogden, M. M. Steinbugler, and T. G. Kreutz, *J. Power Sources* 79, 143 (1999).
2. J. M. Ogden, *Phys. Today* 55, 69 (2002).
3. L. Schlapbach, *MRS Bull.* 27, 675 (2002).
4. R. S. Irani, *MRS Bull.* 27, 680 (2002).
5. A. Domashenko, A. Golovchenko, Yu. Gorbatsky, V. Nelidov, and B. Skorodumov, *Inter. J. Hydrogen Energ.* 27, 753 (2002).
6. E. C. Walter, R. M. Penner, H. Liu, K. H. Ng, M. P. Zach, and F. Favier, *Surf. Interf. Anal.* 34, 409 (2002).
7. J. Kim, B. P. Gila, G. Y. Chung, C. R. Abernathy, S. J. Pearton, and F. Ren, *Solid State Electron.* 47, 1069 (2003).
8. W. Shin, M. Matsumiya, N. Izu, and N. Murayama, *Sens. Actuators B* 93, 304 (2003).
9. X. Bevenot, A. Trouillet, C. Veillas, H. Gagnaire, and M. Clement, *Sens. Actuators B* 67, 57 (2000).
10. N. Maffei and A. K. Kuriakose, *Sens. Actuators B* 98, 73 (2004).
11. S. Shukla, L. Ludwig, C. Parrish, and S. Seal, *Sens. Actuators B* 104, 223 (2005).
12. S. Shukla, S. Seal, L. Ludwig, and C. Parish, *Sens. Actuators B* 97, 256 (2004).
13. S. Shukla, S. Patil, S. C. Kuiry, Z. Rahman, T. Du, L. Ludwig, C. Parish, and S. Seal, *Sens. Actuators B* 96, 343 (2003).
14. S. Seal and S. Shukla, *JOM* 54, 35 (2002).
15. C. Xu, J. Tamaki, N. Miura, and N. Yamazoe, *Sens. Actuators B* 3, 147 (1991).
16. G. Sakai, N. S. Baik, N. Miura, and N. Yamazoe, *Sens. Actuators B* 77, 116 (2001).
17. D. D. Vuong, G. Sakai, K. Shimanoe, and N. Yamazoe, *Sens. Actuators B* 103, 386 (2004).
18. K. H. Cha, H. C. Park, and K. H. Kim, *Sens. Actuators B* 21, 91 (1994).
19. W. J. Moon, J. H. Yu, and G. M. Choi, *Sens. Actuators B* 87, 464 (2002).
20. N. Yamazoe, *Sens. Actuators B* 5, 7 (1991).
21. V. A. Chaudhary, I. S. Mulla, and K. Vijayamohanan, *Sens. Actuators B* 50, 45 (1998).
22. S. Shukla, R. Agrawal, L. Ludwig, H. Cho, and S. Seal, *J. Appl. Phys.* 97, 054307 (2005).
23. B. I. Prenitzer, L. A. Giannuzzi, K. Newman, S. R. Brown, R. B. Irwin, T. L. Shoftner, and F. A. Stevie, *Metall. Mater. Trans. A* 29, 2399 (1998).
24. J. Ding, T. McAvoy, and R. E. Cavicchi, *Sens. Actuators B* 77, 597 (2001).
25. S. Shukla and S. Seal, *Sens. Lett.* 2, 73 (2004).
26. S. Shukla and S. Seal, *Sens. Lett.* 2, 125 (2004).
27. S. Shukla and S. Seal, *Sens. Lett.* 2, 260 (2004).
28. N. S. Baik, G. Sakai, N. Miura, and N. Yamazoe, *Sens. Actuators B* 63, 74 (2000).
29. M. Sriyudthsak, L. Promsong, and S. Panyakeow, *Sens. Actuators B* 13–14, 139 (1993).
30. G. K. Mor, M. A. Carvalho, O. K. Varghese, M. V. Pishko, and C. A. Grimes, *J. Mater. Res.* 19, 628 (2004).

Received: 8 July 2005. Accepted: 12 July 2005.